Master's Thesis

Master's Programme in Nuclear and Particle Physics
Department of Physics, University of Jyväskylä

Academic Year 2017/2018

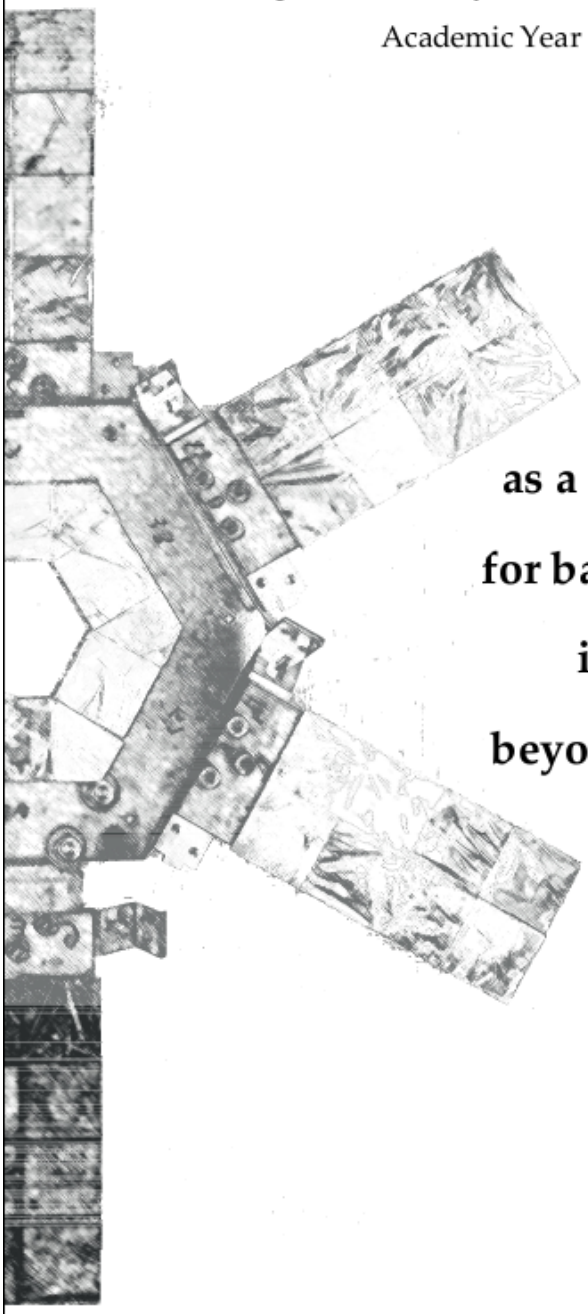

Test of JYUTube as a veto detector at MARA for background suppression in nuclear spectroscopy beyond the proton drip line

Author:

LEANDRO SOTTILI

Supervisor:

JUHA UUSITALO

Co-Supervisor:

JAN SARÉN

23rd July 2018

UNIVERSITY OF JYVÄSKYLÄ

To proff. Grazia Bartalini, Giuseppe Belfi,
Paolo Maurenzig and Gabriella Pinto

Abstract

Sottili, Leandro
Test of JYUTube as a veto detector at MARA for background suppression in nuclear spectroscopy beyond the proton drip line
Master's thesis

Department of Physics, University of Jyväskylä, 2018, 49 pages.

At JYFL-ACCLAB a Mass Analysing Recoil Apparatus (MARA) was built to perform nuclear spectroscopy of exotic nuclei with N=Z in the region A∼80 created via fusion evaporation reactions at low energies (3-6 MeV/u). Fusion recoils are collected with a detector system placed on the focal plane of MARA.

A limit of this technique is the presence of unwanted masses/isobars, created in the reactions, that reach the focal plane. One way to reduce this source of background is to use a detector as a veto at the target position to select and to exclude at the focal plane the unwanted products. For this purpose JYUTube was installed at MARA and tested with the ^{78}Kr+^{96}Mo $\rightarrow$ ^{174}Pt* reaction. In this test, the JYUTube showed an efficiency of 65% for 1 proton channel suppression and 80% for 2 protons channel suppression.

Keywords: JYUTube, MARA, JYFL-ACCLAB, proton-rich nuclides, proton drip line

Contents

Introduction and Motivation

The study of nuclear structure is nowadays focused on nuclei far from the stability, called exotic nuclei, as, for example, the proton-rich nuclides. In order to perform measurements of these nuclides the development of facilities and detection arrays has been carried out in several laboratories, among others JYFL in Jyväskylä. A complete review on the topic is [1].

In this field, one region of interest in recent experimental nuclear physics is the nuclear spectroscopy in the region along the N=Z line above the mass number 60.

In order to produce and study the nuclei in this region, MARA (Mass Analysing Recoil Apparatus) separator was built at the Accelerator Laboratory of Jyvaskylä (JYFL-ACCLAB) in 2016. In a typical experiment, two stable nuclei are fused together in the target chamber and an unstable nucleus is created. Afterwards light particles (neutrons, protons and α nuclei) are evaporated and residual nuclei are focused at the focal plane and implanted in a Double-side silicon detector (DSSD) placed at the end of the beam line. Typical products of decays of fusion recoils that can be studied at MARA are:

- prompt γ rays at the target position;
- α emissions and proton emissions of implanted nuclides;
- γ rays of implanted nuclides[1].

This method of measurement is named Recoil Decay Tagging (RDT).

However, even though MARA is a mass separator, one of the limitation is the unlikelihood to separate isobars. The collection of unwanted isobars, or masses in general, combined with random correlations at the focal plane is a source of background for the measurements.

[1]Detection of γ rays after the implantation is particularly important for the study of the isomeric states.

Possible improvements to enhance the fusion recoil selectivity and to overcome this limitation are:

- to increase the pixellation of the implantation detector to reduce the random correlation rate;
- to identify the β particles emitted from the implanted fusion recoils;
- to improve the mass selectivity of the electromagnetic elements of the separator;
- to detect the evaporated charged particles at the target position to tag the reaction channel.

The present master's thesis work is focused on the last improvement. For this purpose a Jyväskylä-York Universities Tube (JYUTube) detector array was created in a collaboration between the University of Jyväskyla and the University of York. JYUTube was specifically designed and assembled for the target chamber of MARA beam line with the aim to tag charged particles emitted after the formation of the compound nucleus at the target position.

JYUTube performances were tested with the reaction ^{78}Kr+^{96}Mo $\rightarrow$ ^{174}Pt* at MARA in November 2017 with the purpose to measure the efficiency to tag charged particles evaporation reaction channels and veto them out to identify the pure neutrons evaporation channel and its products at the focal plane. Results of the test are presented and discussed in this thesis work.

One of the research interest of MARA collaboration, the β-delayed proton emission, as well as some basic background information are given in chapter one. The experimental apparatus used in this work is presented in chapter two. Third chapter is on the set up and measurements to test the efficiency of the JYUTube to tag the evaporated charged particles at the target position.

Chapter 1

Theoretical background

In this chapter some useful basics in nuclear physics are introduced. In section 1.1 the β-delayed proton emission is presented, in section 1.2 basic concepts of fusion evaporation reactions are given. Section 1.3 is on general properties of radiation detectors and last section is focused on organic scintillators.

1.1 Nuclear stability and β-delayed proton emission

The atomic nucleus is a many body system composed of nucleons, neutrons and protons, interacting through strong (α), weak (β) and electromagnetic (γ) interactions. One relevant mechanism to study these interactions is the nuclear decay. At the present knowledge about 3300 nuclides have been studied, a total of 253 nuclides have not been known to decay, all the others decay.

A clear organization of radioactive decay behaviour can be made using the chart of nuclides, where all nuclides are inserted based on their atomic number (number of protons, Z) and neutron number (N). The mass region of around A$\sim$80 is reported in fig. 1.1.

For mass number[1] A<40 the stable nuclei have basically the same number of neutrons and protons (N=Z), above it the $\frac{Z}{N}$ ratio decreases. This trend is explained with the necessity to enlarge the dimension of the nucleus as the coulomb repulsion among protons increases. In A<100 region the nuclides with a higher $\frac{Z}{N}$ than stable ones decay via β^+ decay or electron capture, on the contrary nuclides with a lower $\frac{Z}{N}$ decay via β^- decay. Above A=100 nuclei can also decay via α emission or spontaneous fission.

[1] Mass number is defined as A=N+Z.

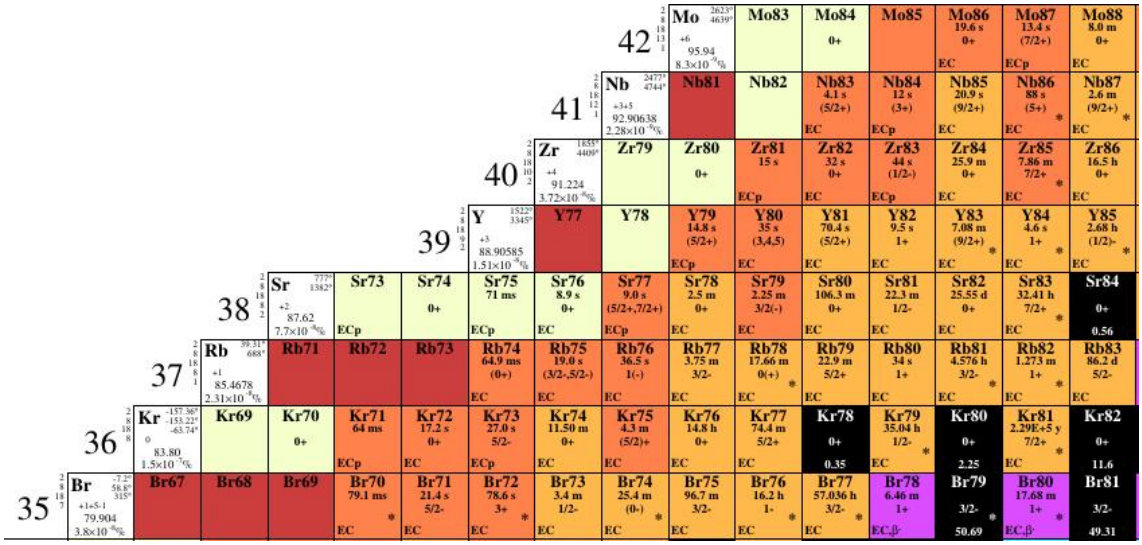

Figure 1.1. Detail of the chart of nuclides for the proton drip line around masses A∼80 from the LUND/LBNL Database [2].

If we consider nuclei with $\frac{Z}{N}$ far from the stable nuclei another decay mechanism can occur: single nucleon decay. In particular, in a same mass region, nuclides with $\frac{Z}{N}$ higher respect to the stable nuclei can decay via single proton emission. In a similar way, for $\frac{Z}{N}$ lower, single neutrons can be emitted. The region where this single proton (neutron) decay occurs is called proton (neutron) drip line. One particular case is the β-delayed proton emission, where a prompt proton is emitted after a β^+ decay of its precursor.

Since, far from stability, the separation energies of the last nucleon becomes smaller and the isobaric mass difference increases, population of proton unbound states via β decay process is favoured. When the β^+ decay is followed by a proton emission, several nuclear spectroscopic information can be achieved. This process has been observed first in Dubna in 1962 and afterwards studied at Brookhaven, Berkeley and ISOLDE. A complete review on β-delayed particle emission is [3].

For example, one of the proposals of MARA group is to study the β-delayed proton emission of ^{77}Zr [4]. The production of this isotope was planned to be obtained through a fusion evaporation reaction and it is expected ^{77}Zr should have a strongly favoured β decay branch to proton unbound isobaric analogue state in ^{77}Y. Further, the energy measurement of the following prompt emitted proton to ground or low-lying excited states of ^{76}Sr could be used to calculate, through Coulomb Displacement Energy method [5], the mass of the β decaying precursor ^{77}Zr.

1.2 Fusion evaporation reactions

According to Krane [6], a nuclear reaction can be written as

$$\mathrm{a} + \mathrm{X} \longrightarrow \mathrm{Y} + \mathrm{b}, \tag{1.1}$$

where nuclei a and X react, for example a projectile and a fixed target, and b and Y are the reaction products. Even though an univocal categorisation of nuclear reactions is not present in literature, the main categories of reaction by mechanisms can be divided in:

- *scattering process*, in which incoming and outgoing particles are the same, however the final states of products can be either the ground states (elastic scattering) or excited states (inelastic scattering);
- *direct reactions*, in which some (but not all) nucleons are exchanged between reacting particles;
- *compound nuclear reactions*, when the incoming nuclei fuse together before evaporations of nucleons or particle ejection takes place.

The formation of a compound nucleus can be obtained via fusion evaporation reaction, for example sending a monoenergetic ion beam on a fixed target. In this process two nuclei merge together (fusion) then, after the equilibrium process takes place, particles (evaporation) are ejected and γ rays are emitted.

It worth to mention here that the properties of the ejected particles depends exclusively from the compound nucleus and not from the properties of the colliding nuclei. Typical formation time of compound nuclei is 10^{-22} seconds, evaporation of particles takes place in a time scale of 10^{-20} seconds.

In order the fusion evaporation reaction takes place

- the beam energy has to be sufficient to overcome the Coulomb barrier;
- the two nuclei have to experience head on collision (small impact parameter).

A first estimation of the energy required to fuse two nuclei can be done considering the Coulomb barrier acting between them. The repulsive potential is given by

$$V_C = \frac{Z_a Z_X e^2}{4\pi\varepsilon_0 \mathrm{R}}, \tag{1.2}$$

where R is the distance that is needed to overcome. For a first approximation it can be used the sum of the two radii

$$\mathrm{R} = r_0({A_a}^{1/3} + {A_X}^{1/3}), \tag{1.3}$$

and combining together 1.2 and 1.3

$$V_C = \frac{Z_a Z_X e^2}{4\pi\varepsilon_0 r_0({A_a}^{1/3} + {A_X}^{1/3})}, \tag{1.4}$$

However, for a more realistic estimation, angular momenta effects have to be considered as presented from Bass [7].

A compact form to write a fusion evaporation reaction is

$$\mathrm{X(a,b)Y}, \tag{1.5}$$

where b are the evaporated particles.

The products of fusion evaporation reactions are not univocally determined, but rather many combinations, named channels, are possible. For example, if we consider the reaction $^{40}\mathrm{Ca}(^{40}\mathrm{Ca}, 3\mathrm{n})^{77}\mathrm{Zr}$, possible reaction channels are:

$$\begin{aligned}
^{80}\mathrm{Zr}^* &\rightarrow^{77} \mathrm{Zr}^* + 3\mathrm{n} && (1.6)\\
&\rightarrow^{77} \mathrm{Y}^* + \mathrm{p} + 2\mathrm{n} && (1.7)\\
&\rightarrow^{77} \mathrm{Sr}^* + 2\mathrm{p} + \mathrm{n} && (1.8)\\
&\rightarrow^{74} \mathrm{Rb}^* + \alpha + \mathrm{p} + \mathrm{n} && (1.9)\\
&\rightarrow^{74} \mathrm{Sr}^* + \alpha + 2\mathrm{n} && (1.10)\\
&\rightarrow^{78} \mathrm{Zr}^* + 2\mathrm{n} && (1.11)
\end{aligned}$$

Furthermore, a channel of the reaction can be favoured setting the energy of the beam. For example, to calculate the beam energy for three neutrons evaporation channel, we have to consider:[2]

- the neutron separation energies from the compound nucleus up to the nucleus of interest;
- the kinetic energy of the evaporated neutrons (typically $\sim 3 - 4$ Mev/u).
- the Q-value of the reaction.

Afterwards, in order to set the energy of the beam, the energy have to be calculated in the laboratory frame. The relationship between the energy in the laboratory frame E_{lab} and in the centre of mass frame E_{com} is

$$E_{com} = \frac{m_a}{m_X + m_a} \cdot E_{lab}, \tag{1.12}$$

Moreover, because the impact parameter is not zero, scattered particles (both target and projectile) are always present. A study of the angular and the energy distributions of the evaporated particles goes beyond the purpose of this thesis, however to have an estimation, the PACE4 [8] simulation program can be used. Furthermore, with LISE++ software [9], an estimation of the energy of the scattered particles from both the beam and the target can be done.

[2]The energy to overcome the Coulomb repulsion has still to be considered a lower limit for energy calculation.

If we consider a fusion evaporation reaction with both projectile and target being stable, it is foreseeable to create proton rich nuclides. In addition, evaporating neutrons from the compound nucleus drives the products towards the proton drip line.

1.3 Generality on radiation detectors

To be detected, the radiation needs to interact with material generating an electrical signal that can be acquired and analysed at the end of the detection process. A device that measures the presence of radiation is called radiation detector.

An ideal radiation detector should be capable to:

- interact with all impinging radiation registering the interaction (high efficiency);
- produce a high amplitude output signal once radiation impinge on it (high sensitivity);
- produce an output signal linearly proportional to the energy of the hitting radiation (linear response);
- distinguish clearly close lying energies (high energy resolution).

No one type of detector possesses all these properties, but each detector is rather designed specifically to improve some of these properties.

According to the literature [10],[11], two different efficiencies are usually referred to a detector, the absolute efficiency

$$\epsilon_{abs} = \frac{\text{event registered on the detector}}{\text{event emitted from sources}}, \tag{1.13}$$

and the intrinsic efficiency

$$\epsilon_{int} = \frac{\text{event registered on the detector}}{\text{event impinging on the detector}}, \tag{1.14}$$

They are related each other with the geometric efficiency, proportional to the solid angle covered by the detector. For example, for an isotropic source, $\epsilon_{int} = \epsilon_{abs}\frac{4\pi}{\Omega}$ where Ω is the solid angle covered by the detector.

The energy resolution is defined as

$$\Delta\mathrm{E} = \frac{\mathrm{FWHM}}{\mathrm{E}}, \tag{1.15}$$

typically given in percentage.

At JYFL-ACCLAB three main types of detectors are currently used: gas detectors, semiconductor detectors and scintillator detectors.

In gas detectors the hitting radiation creates electron-ion pairs. The charges created are collected applying external electric fields. Gas detectors can be used in different modes, for example as proportional counters, where the initial charge generated by the interaction of the radiation is linearly amplified, or as Geiger-Mueller counters, in which all the outcoming signals have the same amplitude despite the initial creation by using very high electric fields.

Semiconductor detectors have been created to have a high number of charge carriers created when radiation impinge on them, and thus to have high energy resolution. In semiconductor materials free electrons and holes are created as the ionizing radiation impinges, a fraction of electrons passes from the valence band to the conduction band and are collected through an external electric field. Materials typically used are silicon and germanium.

In scintillator detectors electrons that form the output signal are decoupled from the electrons produced by the impinging radiation. In order to have an high output signal scintillating materials are coupled with Photomultiplier devices (PMT), such as Phototubes or Silicon Photomultipliers (SiPMs). The main steps of the detection process are:

- the impinging radiation interacts with the material producing the excitation of the atomic electrons;
- prompt light is emitted in the visible range due to the de-excitation of the atomic electrons;
- the light is collected[3] and converted to electrons by a photosensitive material;
- electrons are multiplied by a Photomultiplier (PMT) forming the output signals.

There are two main groups of scintillator detectors: inorganic scintillators and organic scintillators. The first ones have a better energy resolution, while the second type has a faster output. For all kind of detectors, an important role is performed by the front-end electronics and the signal shaping electronics. Further reading are Knoll [10] and Leo [11].

[3]Transparency to its own scintillation light is also required for good light collection.

1.4 Organic scintillator detectors

The light emitted from an organic scintillator is related to the energetic level structure in organic molecules that presents a complex structure of triplet and singlet states as well as vibrational and rotational substates. Referring to figure 1.2, due to an energy gap between substates of S_0 levels of the order of 0.15 eV and a spacing of 3-4 eV between S_0 and S_1, since the average thermal energy at room temperature is 0.025 eV, almost all electrons are in the S_0 singlet state.

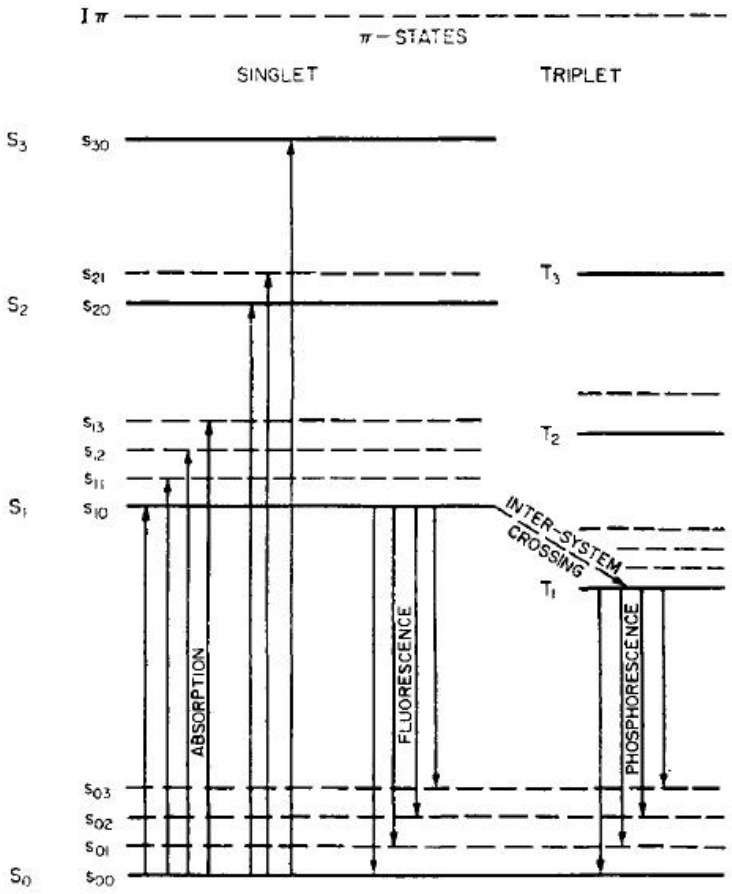

Figure 1.2. Sketch of energy levels of an organic molecule from Birks [12]. Absorption/emission effects are also shown.

When a radiation impinges on the material and releases energy it may excite or either ionize the molecules. The molecular electrons may de-excite in three ways:

- from one singlet to another, with typical time of ns, called fluorescence;
- from one triplet to a singlet, called delayed fluorescence;
- from one singlet to a triplet in the time scale of ms, called phosphorescence.

Other mechanisms to de-excite molecular electrons not related to the impinging radiation, for example de-excitation induced by thermal energy, are possible. These phenomena are typically indicated as quenching.

According to Birks [12], the light output $\frac{dL}{dx}$ is related to the energy loss $\frac{dE}{dx}$ through the formula (known as Birks's formula):

$$\frac{dL}{dx} = \frac{\mathrm{S}\frac{dE}{dx}}{1 + kB\frac{dE}{dx}}, \tag{1.16}$$

where kB is a proportionality constant containing the quenching effects that can be adjusted fitting the experimental data.

A large variety of organic scintillators are nowadays available, for an exhaustive list see Knoll [10], p. 226 and following. In this master's thesis work plastic scintillators have been used.

Chapter 2

Experimental apparatus

At JYFL-ACCLAB are located two beam lines for nuclear spectroscopy as well as one beam line for nuclear reaction studies, a beam line for industrial applications and a beam line for ISOL (Isotope Separation On Line) method [13].

In this chapter the instruments used for the test of JYUTube are described. First the accelerator facility is presented in section 2.1, afterwards MARA beam line and the JYUTube detector array are introduced and described respectively in sections 2.2 and 2.3.

2.1 Brief overview of the K130 cyclotron and ion sources

One of the ranges of energy to perform modern experiments of nuclear spectroscopy is between 3 MeV/u and 8 MeV/u, the accelerator capable to reach these energies present at JYFL-ACCLAB is the K130 cyclotron [14].

In order to create ion beams for K130 three different ion sources can be used: LIISA, a plasma source for the production of H and D ions and two Electron Cyclotron Resonance (ECR) ion sources, named ECR1 and ECR2. Using LIISA electrons are produced heating a filament and hydrogen isotopes are negatively ionized in the plasma. Electrons are stripped at the extraction of the cyclotron with a carbon foil and afterwards positive ions are delivered to the beam lines. In ECR sources [15] electron plasma is created using strong magnetic fields produced in coils, in addition microwaves at the same frequency of the electrons are overlapped. With this mechanism, electrons are able to ionize the injected gas and to further ionize ions reaching high charge states. Typical ion energies at the output of the ion sources are tens of keVs.

Ion beams are carried out through injection lines and, before being injected in the K130 cyclotron, compressed with a buncher. In the K130 cyclotron the magnetic field increases with radius in order to maintain the frequency of the ions constant (isochronous cyclotron). Main components of this accelerator are the main coils and the 15 correction coils that define the magnetic field, three spiral sectors to focus the beam and the two dees of the RF system to pulse the beam and to accelerate it while it pass the gaps between the four dees.

Inside the cyclotron ions bend according with the Lorentz force, accelerated particles are extracted and reach the measurement stations[1]. The maximum energy reachable with K130 is given by the formula

$$E = 130\frac{Q^2}{A}\ [\text{MeV}], \tag{2.1}$$

where Q is the charge state and A is the mass number. The mass resolving power of the K130 cyclotron is around 0.02% [16]. Further information can be found in Heikkinen's article [17].

2.2 MARA beam line

The MARA beam line was built to perform nuclear spectroscopy for N≈Z nuclides below A=100 starting from the fusion of stable nuclei. In order to separate fusion recoils from other particles, and residues of the reactions each others, it was decided to build a vacuum mode recoil mass separator. Since MARA is capable to separate residues, it can be also considered a spectrometer. The main components of MARA are:

- the target chamber;
- the magnetic quadrupole triplet;
- the electrostatic deflector;
- the magnetic dipole;
- the detector system at the focal plane.

The entire separator is approximately 7 meters long from target chamber to collection detector, a sketch is presented in fig.2.1.

The target chamber is equipped with a rotating wheel connected outside with a manipulator in order to change target during an experiment without need to vent the chamber.

[1] Along the ejection beam lines are located several diagnostic elements as beam profile monitors and Faraday cups.

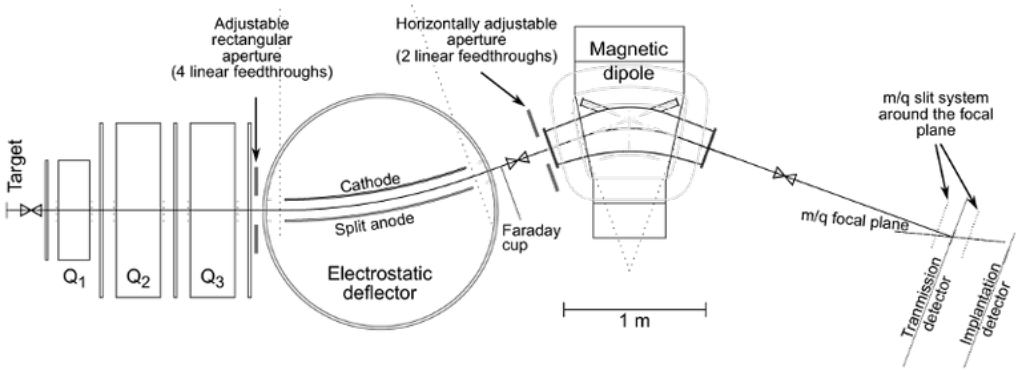

Figure 2.1. Schematic view of MARA beam line from [18].

Since both the beam-target interaction area and the region where residues are collected can be considered point-like compared with the length of the beam line, the overall ion optical focus is point to point focusing system. For this reason after the target chamber, where the reaction takes place, the diverging products are focused by the quadrupole triplet.

In order to describe how the electrostatic deflector and the magnetic dipole act on the beam, it is useful to introduce the electrostatic rigidity $\chi_E = E\rho$ and the magnetic rigidity $\chi_B = B\rho$, where ρ is the bending radius of the ions under the effect of the fields. For non relativistic energies, if the magnetic field is homogeneous and perpendicular to the velocity of the particles

$$\chi_B = \frac{mv}{q}. \tag{2.2}$$

Similarly, if the electric field is perpendicular to the velocity of the ions

$$\chi_E = \frac{2E_k}{q}. \tag{2.3}$$

Starting from 2.3 and 2.2, the electrostatic deflector of MARA separates the ions according to the formula

$$V(E_k) = \frac{E_k[MeV]}{q[e]} \ln(\frac{\mathrm{R}_2}{\mathrm{R}_1}) \text{ [MV]}, \tag{2.4}$$

where $V(E_k)$ is voltage between the two plates, E_k is the kinetic energy of the ions and R_1 and R_2 are the inner and outer radii of the electrostatic deflector; while the magnetic dipole bends the remaining recoils according to the equation

$$\chi_B = 0.1527 \cdot \frac{\sqrt{2E_k[MeV] \cdot m_0[u]}}{q[e]} \text{ [Tm]}, \tag{2.5}$$

where χ_B is the magnetic rigidity, m_0 is the mass of the recoil and q is its charge state. In addition, some slits systems are present along the beam line to improve the selectivity at the focal plane. A complete description can be found in Dr. Sarén's PhD Thesis [19].

The electric and magnetic fields focus the charged particles such that there is an energy focusing at the focal plane, where the detector system is placed [2]. Thus, the MARA is a double (energy and angular) focusing device.

The detector system of MARA consists of:

- a Multi-Wired Proportional Counter (MWPC), a position sensitive gas detector filled with isobutane, with one array of wires in the central region (anode) and two on the sides (cathode), used as transmission detector;
- the Double-sided Silicon Strip Detector (DSSD), an highly pixelated silicon detector, in which the ions are implanted[3];
- four clover Germanium detectors behind the DSSD detectors.

Once an ion reach the focal plane, its time of flight (TOF) is measured with a time to amplitude converter (TAC) module between the signals in the MWPC and the DSSD, ions are implanted in the DSSD in which, since they are typically not stable, they decay [4]. The mass (over charge) spectrum is obtained from the MWPC. Properties of the α and proton decays can be measured with the DSSD itself, whereas information of γ spectroscopy can be achieved with the clover Germanium detectors. Moreover, other detectors can be added at the focal plane to tag β particles and protons, for example a punch-through silicon detector behind the DSSD.

[2]Typically the focus is inside the transmission detector.

[3]Several DSSD detectors with different thickness and pixel size are available and are chosen depending on the needs.

[4]The time of flight of fusion recoils inside MARA varies according with their mass and energy, however their halflives have to be at least hundreds of ns to reach the focal plane, otherwise they decay in flight.

2.3 JYUTube detector array

The JYUTube detector array tested in the present thesis work consists of 120 cells each one formed by an Eljen EJ200 scintillator glued to a light guide which in turn is glued to a SiPM. In order to maximize the signal from EJ200 scintillator, since it has maximum light emission at 425 nm, it was coupled with a SiPM that has the maximum photon detection efficiency (PDE) for wavelengths between 400 nm and 450 nm, in our case an SMT of the C-series of the sensL company [20]. The main properties of EJ200 scintillator are summarized in table 2.1 and the PDE curve of the SiPM is shown in fig.2.2.

Table 2.1. Specification of Eljen scintillators from reference [21].

PROPERTIES	EJ-200	EJ-204	EJ-208	EJ-212
Light Output (% Anthracene)	64	68	60	65
Scintillation Efficiency (photons/1 MeV e^-)	10,000	10,400	9,200	10,000
Wavelength of Maximum Emission (nm)	425	408	435	423
Light Attenuation Length (cm)	380	160	400	250
Rise Time (ns)	0.9	0.7	1.0	0.9
Decay Time (ns)	2.1	1.8	3.3	2.4
Pulse Width, FWHM (ns)	2.5	2.2	4.2	2.7
H Atoms per cm³ ($\times 10^{22}$)	5.17	5.15	5.17	5.17
C Atoms per cm³ ($\times 10^{22}$)	4.69	4.68	4.69	4.69
Electrons per cm³ ($\times 10^{23}$)	3.33	3.33	3.33	3.33
Density (g/cm^3)	1.023	1.023	1.023	1.023
Polymer Base	Polyvinyltoluene			
Refractive Index	1.58			
Softening Point	75°C			
Vapor Pressure	Vacuum-compatible			
Coefficient of Linear Expansion	7.8×10^{-5} below 67°C			
Temperature Range	-20°C to 60°C			
Light Output (L.O.) vs. Temperature	At 60°C, L.O. = 95% of that at 20°C No change from -60°C to 20°C			

The two most important properties for our purposes are the fast output and the high detection efficiency. The energy response for nuclei is shown in fig. 2.3 and it is lower than for electrons, whereby the amplitude of output signals for electrons is expected to be higher than the amplitude for protons of the same energy.

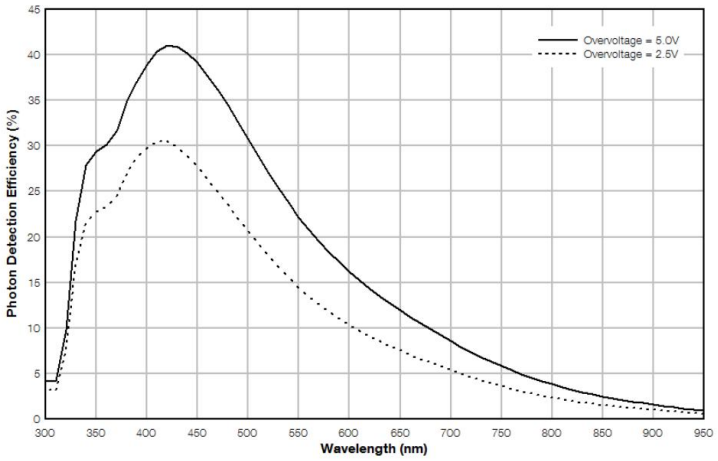

Figure 2.2. Trend of the Photon Detection Efficiency (PDE) with the incoming wavelength from [20].

Moreover, the number of photons produced after the excitation decreases with the mass of the impinging particle, thus signals from α particles are expected to give a lower signal in the energy spectrum of the JYUTube than protons.

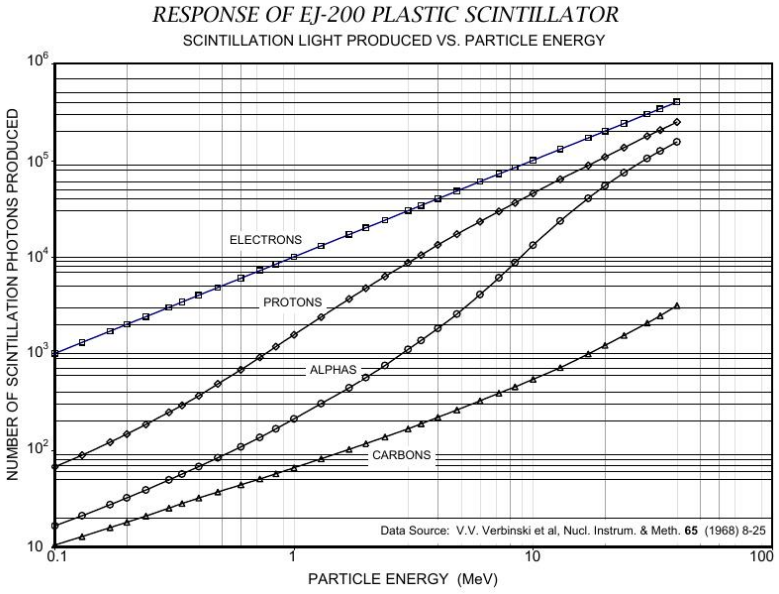

Figure 2.3. Response of EJ200 detector to charged particles from [21].

In addition, also γ rays and neutrons can interact and release energy inside the scintillators. Even though a documentation for the EJ200 detector it is not available, some information about the efficiency for γ rays can be extracted from Kantele [22].

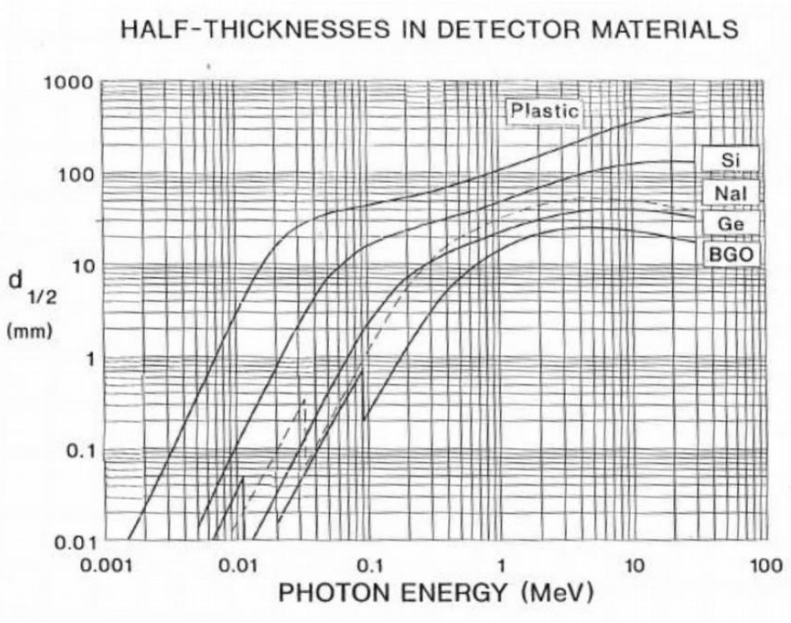

Figure 2.4. Half thickness of detector materials to γ rays from Kantele [22], p.130.

Using the data from fig. 2.4, the transmission can be calculated as

$$I(x) = I_0 2^{\frac{-x}{d_{1/2}}}, \tag{2.6}$$

results for different energies are presented in table 2.2

Table 2.2. Transmitted γ rays in 2 mm thickness for plastic material according to fig. 2.4 and equation 2.6.

Energy (MeV)	Transmission (%)
0.1	97.3
1	98.6
10	99.5

JYUTube has one hundred and eight detectors squared with an area of 20 mm x 20 mm, the last twelve are rhombic shaped. All scintillators are 2 mm thick.

Cells are arranged in 12 panels and two end cups. Each panel is made of two lines of 4 square detectors, end cups are made of 12 scintillators, 6 square and 6 rhombic detectors as presented in fig. 2.5 . This disposition was chosen to maximize the solid angle covered by the JYUTube.

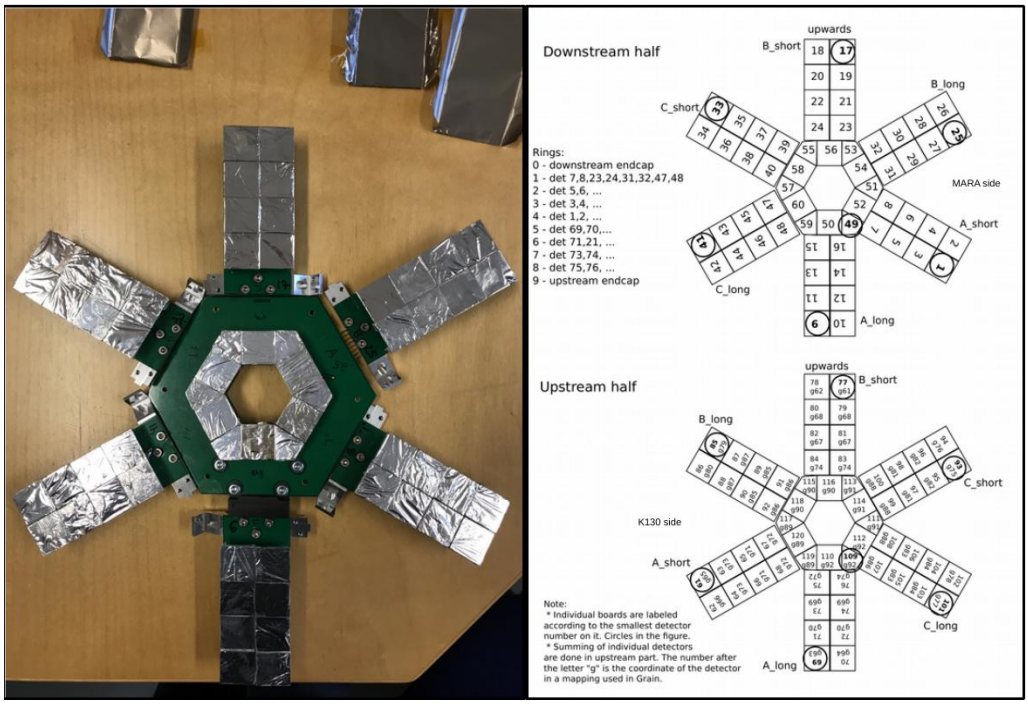

Figure 2.5. Picture of half of the JYUTube partially unmounted (left), sketch of the JYUTube with detectors labelled (right).

Each cell was painted and covered with a silver tape, except for the top of the scintillator that was covered with aluminized Mylar foils [5]. For each SiPM there are two out coming wires (anode and cathode). The SiPMs were mounted onto a Printed Circuit Board (see fig. 2.6) where their signals are collected. Cells were bound to each other with glue. Boards are then supported with brackets.

Figure 2.6. Picture of a single panel of JYUTube held by the author.

The solid angle covered by the JYUTube can be calculated considering each half of the JYUTube as a hollow hexagonal base cylinder with a hexagonal opening. The

[5]The Mylar thickness is 2 μm, the Al coating is less than 1 μm.

solid angle not covered by the detector can be thus estimated as an hexagonal base pyramid that covers a solid angle given by the equation

$$\Omega = 2\pi - 12\arctan(\frac{tan\frac{\pi}{6}}{\sqrt{1+\frac{l^2}{h^2}}}), \tag{2.7}$$

where l is the dimension of the hexagonal side and h is the height of the pyramid. With the values l=20 mm and h=81.5 mm from a Computer Aided Design (CAD) model of the JYUTube, the solid angle covered from the entire JYUTube is ∼97%. In reality this value is overestimated since the two halves cannot be placed in touch in the target chamber due to the necessity to input the target in between.

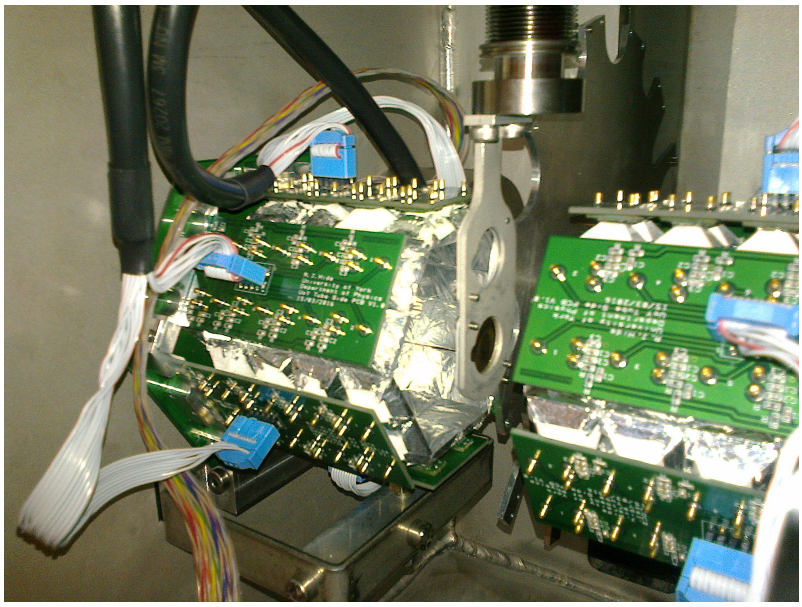

Figure 2.7. Picture of the JYUTube mounted in the target chamber of MARA.

Last, it is worth to mention the range of the protons and α particles in plastic material. An estimation of the average range of these particles can be done using SRIM software [23]. From SRIM simulations the range of the protons varies from 22±1 μm for 1 MeV protons to 4.07±0.16 mm for 20 MeV protons. For α particles the range is between 4.8±1.2 μm (1 MeV) and 1.17±0.04 mm (40 MeV).

Chapter 3

Measurements and Analysis

First, JYUTube was tested with α particles. An ^{241}Am source and a compound source with ^{241}Am and ^{148}Gd (Am-Gd source in the following) were used. Afterwards a ^{207}Bi and ^{60}Co sources to study the response of the JYUTube to β particles and γ rays were also used.

Secondly, JYUTube performances were tested locating it at the target position, a fusion evaporation reaction was run in the mass region 170. Data from JYUTube were collected using Moving Window Deconvolution Algorithm (MWDA) [24] since it was not possible to collect traces with the acquisition system during the experiment. Data were acquired using MIDAS, a data acquisition system developed at Daresbury Laboratory [25].

In those measurements no shaping electronics was used for JYUTube. Data stream from detectors was recorded with commercial Lyrtech VHS-ADC cards, signals were digitized using the field-programmable gate array (FPGA) hardware with a sampling frequency of 100 MHz with 14-bit resolution.

3.1 First tests with α, β and γ sources

Half of the JYUTube was placed in a target chamber and biased with 29.5 V [1]. The sources were mounted in different positions on the rotating wheel, a vacuum around 10^{-2} mbar was created with a roughing pump. Since signal traces were acquired, different signal analyses were performed off-line.

[1] This value was taken from the SiPM data sheet [20]

3.1.1 Test with α sources

The geometry of the JYUTube was divided in rings as shown in fig. 2.5. Energy spectra were created for each ring summing the signals of all detectors in the ring.

Using ^{241}Am source all the spectra from each ring have almost the same shape with the exception of the ring 9, that correspond to the end cup.

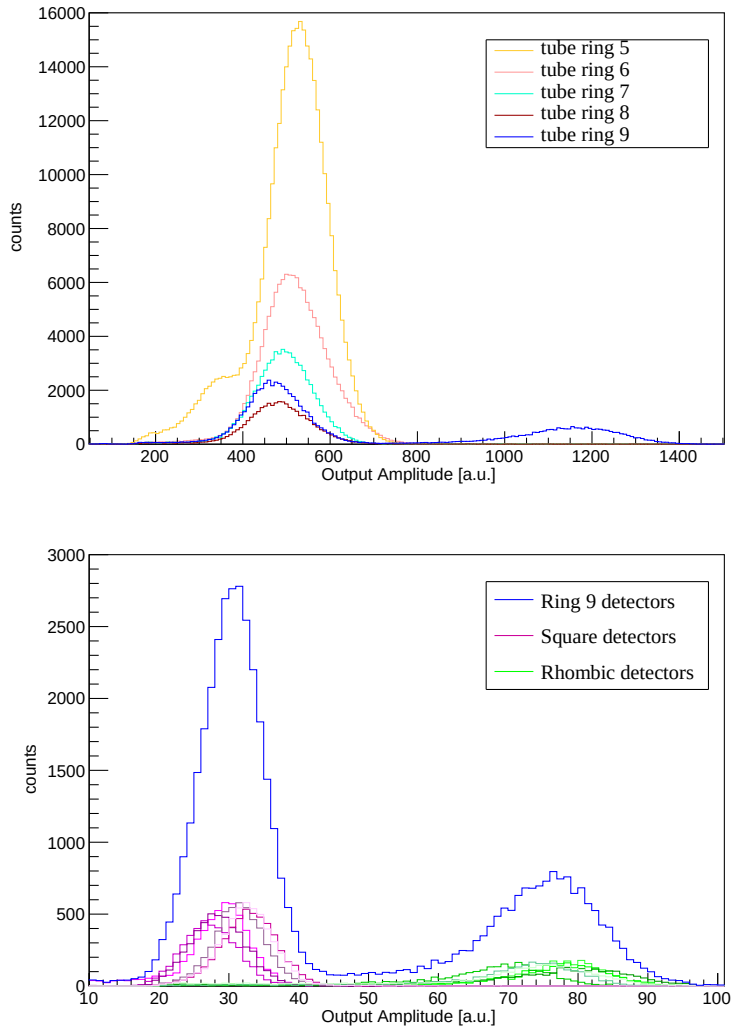

Figure 3.1. Amplitudes of the signals from each ring (top). Amplitudes of signals from the twelve detectors of the end cup (bottom), squares detectors are in violet, rhombic detectors in green.

In this last case, the two peaks in the distribution are related with the two different shapes of the detectors in the end cup: the square detectors emit a signal as the detectors in the barrel, whereas the rhombic detectors have an higher output value (see fig. 3.1). This fact is explicable if we consider that the area of the rhombic

detectors is smaller compared with the area of the square ones, thus the light dispersion in the light guide before photons reach the SiPM is less, hence, considering that the photon-electron conversion of the SiPMs is the same, the amplitude of the output signal is higher.

Afterwards, Am-Gd source was used to study the resolution of the JYUTube. ^{241}Am and ^{148}Gd nuclides emit α particles respectively at 5.486 MeV and 3.183 MeV, the energy spectrum obtained is presented in fig.3.2. Two histograms were created to compare the energy resolution achievable with different type of analyses. The area of signals was compared with the high of the peak of the signals in fig. 3.2(bottom) and with the MWDA in fig. 3.3.

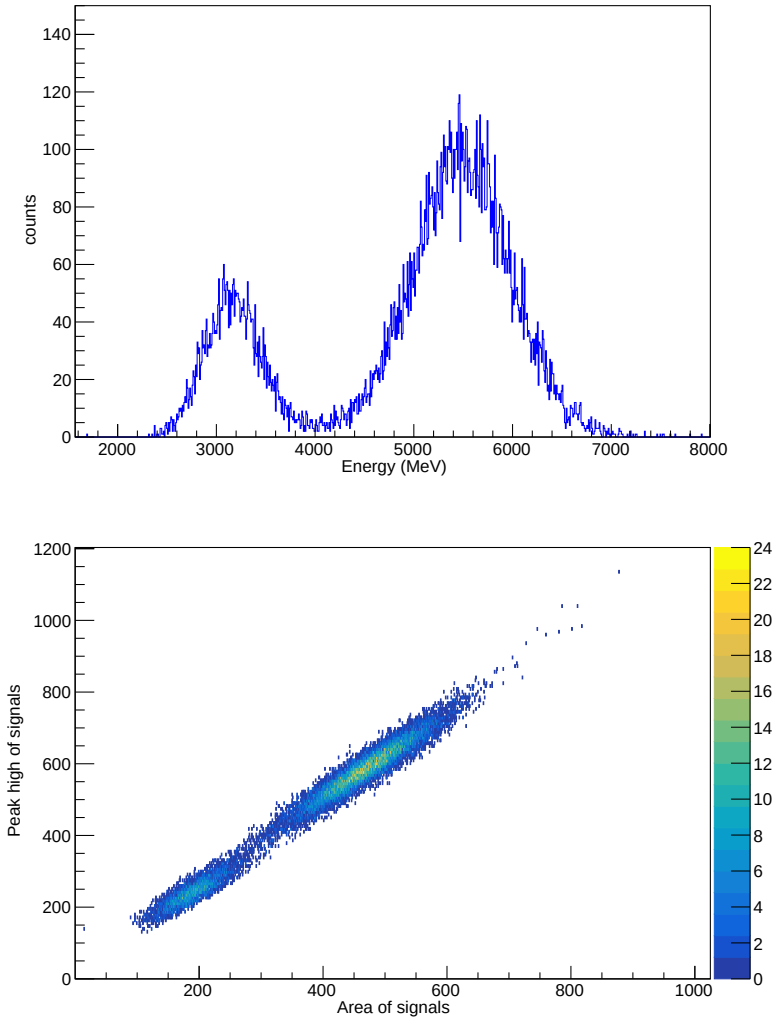

Figure 3.2. Energy spectrum of Am-Gd source from JYUTube using the area of the signals (top), comparison between peak analysis and integral of the signals (bottom). The two peaks at 3.183 MeV (Gd) and 5.486 MeV (Am) are visible.

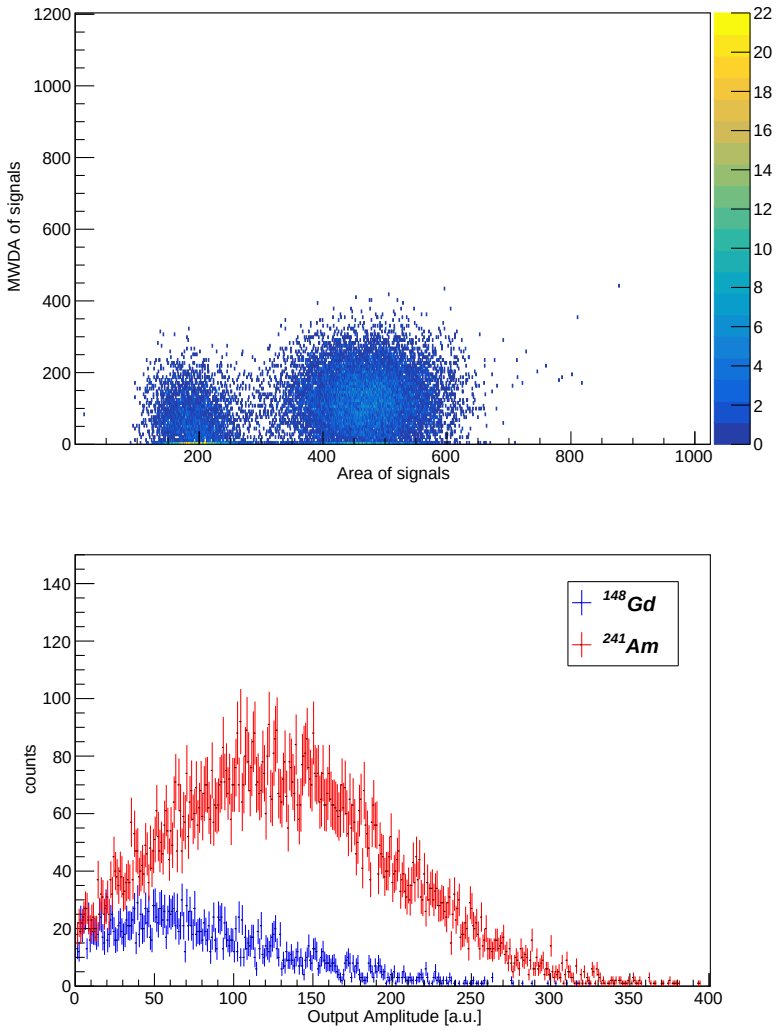

Figure 3.3. Comparison between energy distributions with the area of signals and the MWDA (top), the two peaks are not discernible any more. In the bottom, the distribution with MWDA selecting the source.

As can be seen a resolution of ∼21 % can be achieved with the JYUTube using the area of the signals. On the contrary, as can be seen from fig. 3.3 using MWDA the two peaks are not discernible any more. However, selecting α particles from each nuclides, an increasing trend in average of the distributions with the energy of the α particles was observed.

3.1.2 Test with electrons and γ sources

^{60}Co nuclide has an halflife of $t_{\frac{1}{2}}$=5.37y and emits two prompt γ rays in cascade at 1.173 MeV and 1.332 MeV. The source used had an activity of 12 kBq in January 2006. According with the decay law

$$A(t) = A(0)e^{-\frac{t}{\tau}}, \tag{3.1}$$

the activity in February 2018 was ∼1275 Bq.

From the test with ^{60}Co source, even though the photopeak is not visible, several events were detected. The efficiency to detect γ rays is calculated as the ratio between the counts and the activity and it is ∼ 6.5%.

Moreover a ^{207}Bi source was used to measure the efficiency for conversion electrons detection. The spectrum from detector 77 is presented in fig. 3.4. From the comparison between the spectrum from the Am-Gd source and ^{207}Bi source a higher energy response for electrons respect to α particles is visible. This can be explained with the response curve shown in fig. 2.3. Last, considering the number of signals

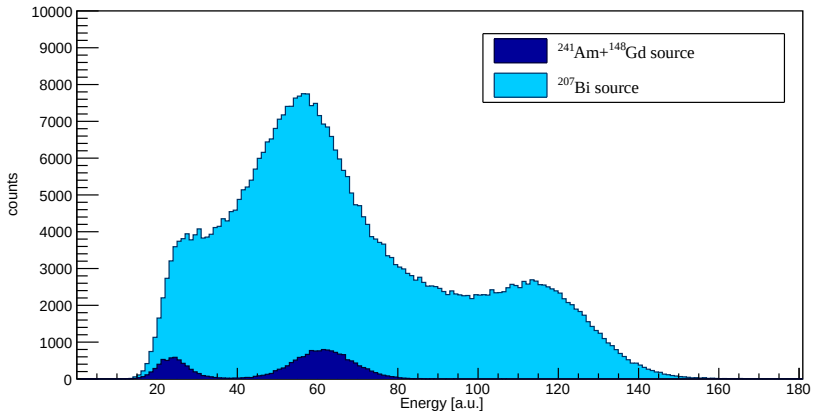

Figure 3.4. Comparison between spectrum from Am-Gd source (blue) and ^{207}Bi source (azure). The energies of the α particles from Am-Gd source are 3.183 MeV and 5.486 MeV, the kinetic energies of the conversion electrons are, among others, 482 keV (1.5% of the cases) and 976 keV (7.0% of the cases) [26].

registered from the JYUTube for each event (called fold number in the following and indicated with FOLD-N), it can be seen that the fold number is higher than

expected. For example in the case of ^{241}Am one FOLD-7 event out of $\sim 5.5 \cdot 10^5$ has been registered, while for the ^{60}Co source FOLD-15 was achieved in two events out of $\sim 2.5 \cdot 10^5$. This circumstance can be explained partially with multiple emissions from the sources and partially with the secondary effect of ionization of molecules of the scintillators and consequent scattering of the electrons inside the JYUTube, that in turn are detected and generate signals.

Other possible causes of this effect can be the electronic cross-talk in the SiPMs and the detection of cosmic muons in coincidence. Moreover, for the ^{241}Am and Am-Gd source the decay schemes envisage emission of γ rays in cascade with the α particles; however, due to the high transmission of γ rays in the scintillators and to the low number of γ rays emitted from the sources, a more detailed analysis was not done in this work.

3.2 Test in A=170 region

In order to measure the efficiency of the JYUTube at MARA a first test in the mass region 170 was planned since in this region unstable nuclides are α emitters with half lives of the order of seconds, whereby fusion recoils are easy to be identified with MARA set up. JYUTube was placed in the target position and SiPMs were biased with 30V. Pressure levels were around 10^{-7} mbar.

3.2.1 Experimental Set up

The fusion reaction planned is

$$^{78}\mathrm{Kr} + {}^{96}\mathrm{Mo} \rightarrow {}^{174}\mathrm{Pt}^{*} \tag{3.2}$$

A foil of ^{96}Mo 500$\frac{\mu g}{cm^2}$ thick was mounted on a rotating wheel as target. ^{78}Kr^{16+} was used from K130 cyclotron with a beam current of 5 pnA[2] and the RF frequency of K130 was set to ∼11 MHz. Beam energy was optimized for 4 neutrons evaporation channel. According with section 1.2 and equation 1.12 the beam energy was set to 390 MeV[3]

By using PACE4 it is possible to estimate the energy distribution of evaporated particles as a function of the angle, for reaction 3.2 at 390 MeV the range of protons is between 1 MeV and 30 MeV, while the maximum energy for the α particles is more than 30 MeV. In addition, due to kinematic reasons, particles that are evaporated forward have an energy distribution, on average, higher than backward (see Appendix B).

[2]A relatively low current was set in order to avoid high rates both for the target and for the detector and acquisition system.

[3]This value of the energy was actually optimized for another experiment with ^{96}Ru target run in parallel.

Moreover, with LISE++ the energy distribution of scattered ^{78}Kr and ^{96}Mo nuclei as a function of the angle can be simulated. As can be seen in fig. 3.5, nuclei scattered forward have the maximum energy (390 MeV) and the energy decreases as we reach the target position.

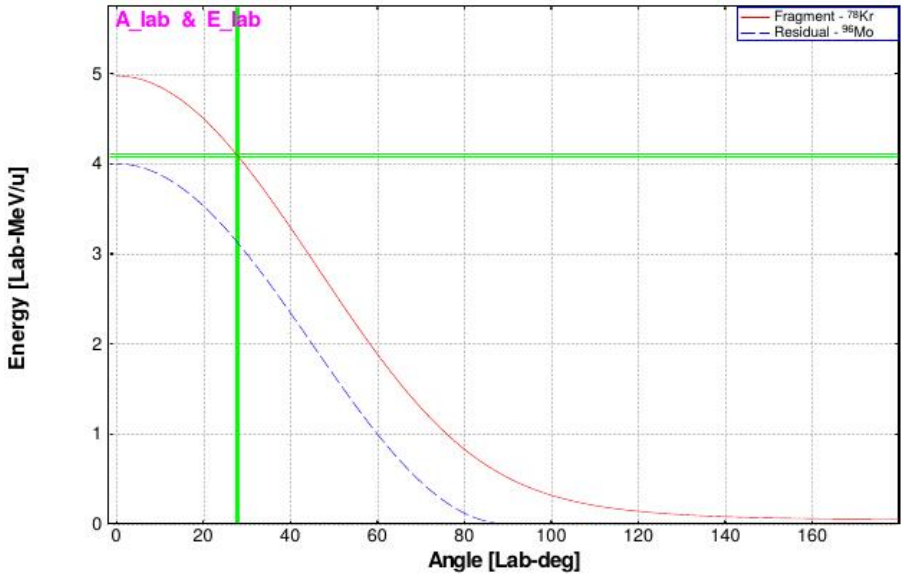

Figure 3.5. Energy of scattered Kr and Mo nuclei as a function of the angle from LISE++ simulations. Target is at 90°.

For these reasons, Ni foils of different thickness were placed on the JYUTube: 20 μm thick foils were placed on the downstream end-cup, 10 μm thick foils on the panels and 5 μm thick foils were placed on the upstream end cup. Calculations are presented in Appendix A.

As already explained in section 1.2 the fusion evaporation reaction 3.2 has many open channels, some examples are:

$$
\begin{aligned}
^{174}\mathrm{Pt}^{*} &\rightarrow^{170} \mathrm{Pt}^{*} + 4\mathrm{n} && (3.3)\\
&\rightarrow^{169} \mathrm{Ir}^{*} + \mathrm{p} + 4\mathrm{n} && (3.4)\\
&\rightarrow^{170} \mathrm{Os}^{*} + 2\mathrm{p} + 2\mathrm{n} && (3.5)\\
&\rightarrow^{169} \mathrm{Os}^{*} + 2\mathrm{p} + 3\mathrm{n} && (3.6)\\
&\rightarrow^{168} \mathrm{Os}^{*} + \alpha + 2\mathrm{n} && (3.7)\\
&\rightarrow^{168} \mathrm{Os}^{*} + 2\mathrm{p} + 4\mathrm{n} && (3.8)\\
&\rightarrow^{167} \mathrm{Os}^{*} + \alpha + 3\mathrm{n} && (3.9)
\end{aligned}
$$

Fusion evaporation recoils were focused in the MWPC to collect at least three charge states; after passing the MWPC, residues were collected on the DSSD detector. The

overall optical system of MARA was set for a reference particle[4] of mass 169 with an energy of 156 MeV and a charge state of 33.5.

3.2.2 Measurements and Data Analysis

Data were collected and analysis was made using GRAIN software [27] and ultimated with ROOT [28]. In order to identify the nuclides their Time of Flight was measured from DSSD and MWPC signals, TOF histogram is presented in fig. 3.6. According

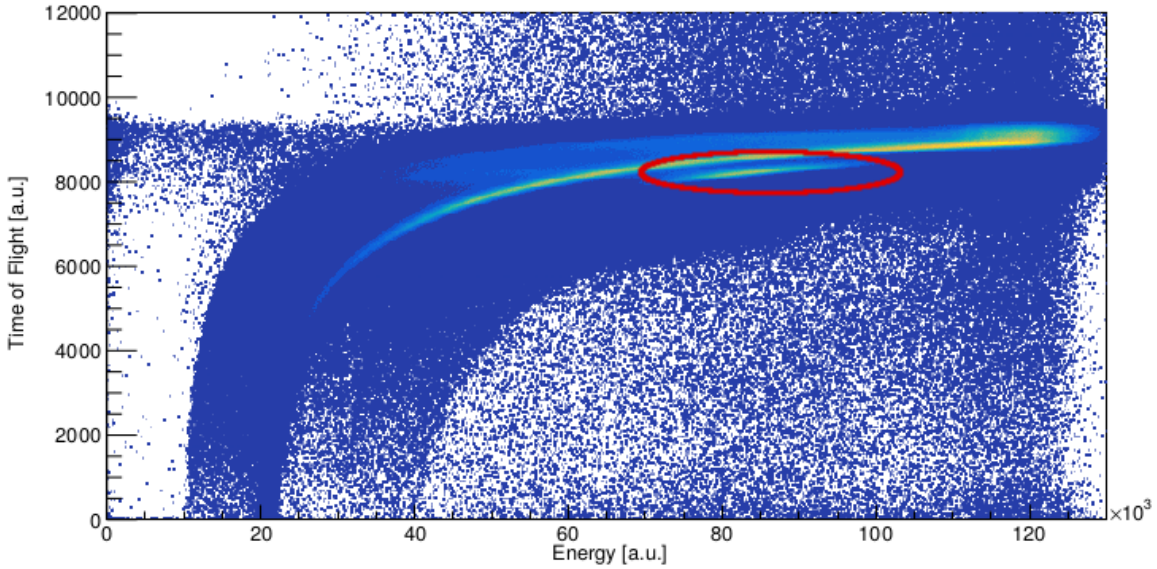

Figure 3.6. Time of flight of ions at the focal plane, fusion recoils are circled in red.

to the TOF formula, particles with the same energy but higher mass have an higher TOF, thus fusion recoils can be selected and separated from scattered nuclei.

Afterwards, the implanted isotopes were identified based on:

- the energies of their α decays in the DSSD, presented in fig. 3.7, centre;
- the lifetimes of the decays, in fig. 3.7, bottom;
- the energies of the daughter's α decays;
- the $\frac{m}{q}$ ratios from the MWPC, shown in fig. 3.7, top.

Lifetimes and energies of the α decays are reported in tab. 3.1, m/q ratios are presented in tab. 3.2. Moreover, an overall picture of the analysis is shown in fig. 3.7.

[4]The reference particle is defined as the particle that has a trajectory on the optical axis, thus its coordinate are always zero.

Table 3.1. Energy of the α particles E_α emitted and lifetimes τ of fusion recoils of the reaction 3.2

NUCLIDE	E_α (MeV)	τ (s)	ln(τ) (s)
^{170}Os	5.443	7.1	2.0
^{169}Os	5.578	3.2	1.2
^{168}Os	5.676	2.1	0.7
^{167}Os	5.836	0.839	-0.2
^{169}Ir	6.105 | 6.005	0.32 | 0.64	-1.1 | 0.4
^{170}Pt	6.550	0.015	-5.0

Table 3.2. Values of m/q ratio from MWPC for nuclides produced during the reaction 3.2 at 390 MeV at MARA. For each isotope, calculated values are on the right, measured values are in the left columns.

CHARGE STATE	^{170}Os		^{169}Os		^{168}Os		^{167}Os		^{169}Ir		^{170}Pt	
31	-	-	5.45	5.40	5.42	5.40	5.39	5.38	-	-	-	-
32	5.31	5.29	5.28	5.28	5.25	5.24	5.22	5.19	5.28	5.29	5.31	5.30
33	5.15	5.14	5.12	5.12	5.09	5.08	5.06	5.06	5.12	5.14	5.15	5.14
34	5.00	4.98	4.97	5.00	-	-	4.91	4.87	4.97	4.98	5.0	5.0

With the results of this analysis it is possible to identify the osmium and iridium isotopes created in the respective channels of the fusion evaporation reaction. Signals were acquired at the target position from the JYUTube in time coincidence any time a fusion recoil was identified with above procedure.[5] For any event, signals from the JYUTube were recorded using MWDA.

[5] A time window of 12 μs was open once a recoil was identified, then a gate of 120 ns was set to reduce the background.

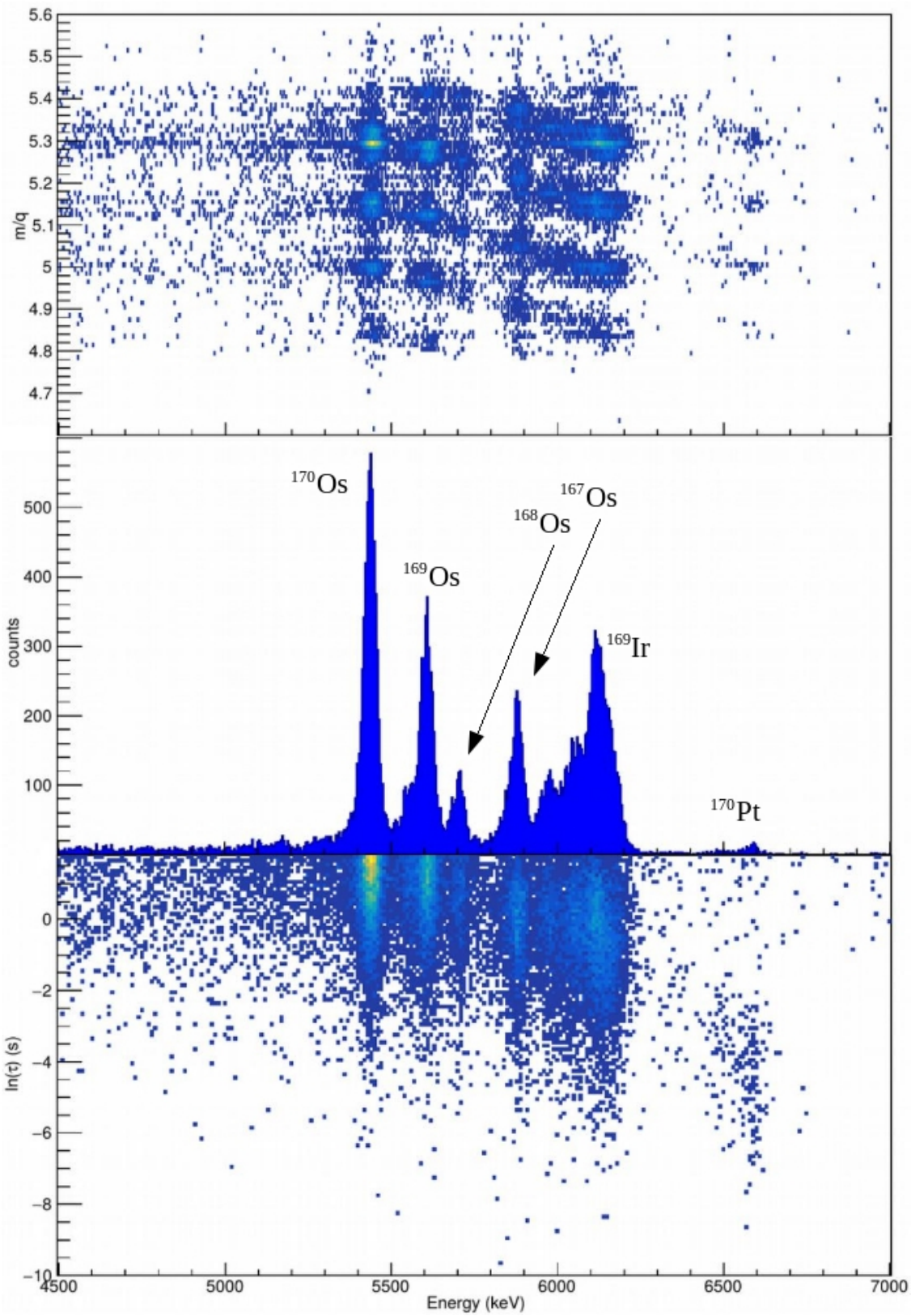

Figure 3.7. Mass over charge values from MWPC (top), energy spectrum of α decays in the DSSD (centre) and lifetimes of fusion recoils (bottom).

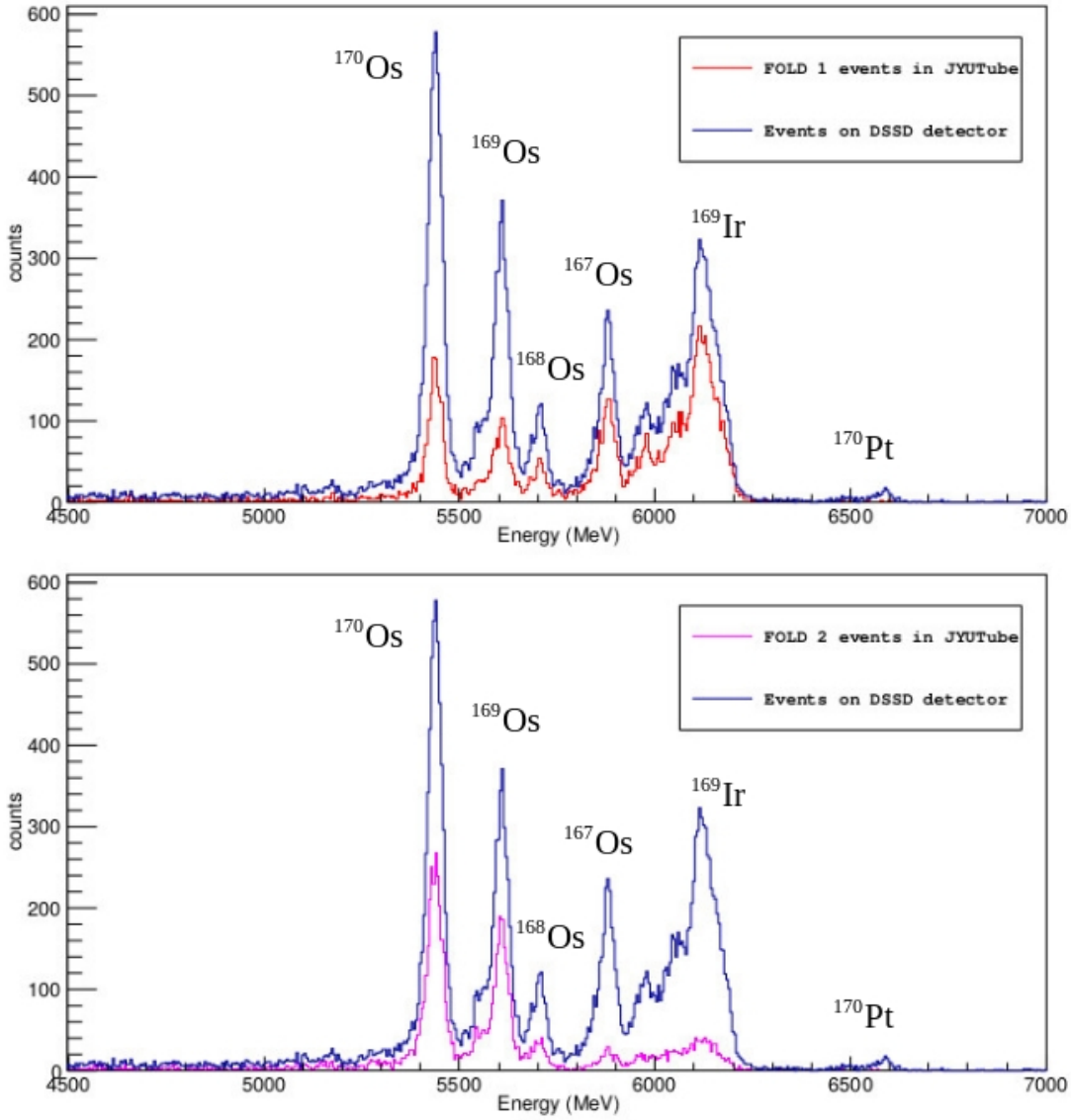

Figure 3.8. Energy spectrum of the α decays from DSSD compared with the energy spectrum of the α decays from DSSD gated on FOLD-1 event(top) and FOLD-2 event(bottom) from JYUTube.

The efficiency of the JYUTube to detect charged particles evaporated at the target position is measured comparing the number of signals from the JYUTube and the number of charged particles emitted in the corresponding reaction channel. For example, for the ^{78}Kr(^{96}Mo, 1p4n)^{169}Ir channel, the emission of one proton occurs, thus this channel is used for the efficiency to detect one particle. On the other hand, the ^{78}Kr(^{96}Mo, 2p2n)^{170}Os and ^{78}Kr(^{96}Mo, 2p3n)^{169}Os are used for the two particles events. The reaction channels corresponding to ^{167}Os and ^{168}Os residues have not been used since both one α nucleus and two protons can be evaporated. Results are presented in fig. 3.8 and table 3.3.

Table 3.3. Number of events registered per FOLD-N in each reaction channel.

RECOIL	TOTAL	FOLD 0	FOLD 1	FOLD 2	FOLD 3	FOLD 4	FOLD >4
^{170}Os	5471	417 *7.62%*	1519 *27.76%*	2527 *46.19%*	815 *14.90%*	155 *2.33%*	38 *0.7%*
^{169}Os	2908	208 *7.15%*	826 *28.40%*	1485 *51.07%*	322 *11.07%*	55 *1.89%*	12 *0.4%*
^{168}Os	820	135 *16.46%*	332 *40.49%*	263 *32.07%*	77 *9.39%*	11 *1.34%*	2 *0.2%*
^{167}Os	2094	605 *28.89%*	1177 *56.21%*	233 *11.12%*	56 *2.67%*	19 *0.91%*	4 *0.2%*
^{169}Ir	5152	890 *17.27%*	3350 *65.02%*	672 *13.04%*	181 *3.51%*	49 *0.95%*	10 *0.2%*
^{170}Pt	142	113 *79.58%*	15 *10.56%*	9 *6.34%*	3 *2.11%*	2 *1.41%*	0 *0%*

The table 3.3 shows an increase of number the FOLD-N events corresponding to the expected number of the charged particles evaporated. For example, for ^{78}Kr(^{96}Mo, 1p4n)^{169}Ir channel FOLD-1 is 65%, while for ^{78}Kr(^{96}Mo, 2p3n)^{169}Os channel FOLD-2 is 51%. However, even in the pure neutron evaporation channel (^{170}Pt residue), events with different FOLD-N have been registered, and it has to be related with the detection efficiency of the JYUTube for de-excitation γ rays and neutrons from the compound nucleus. In addition, also β particles produced during the experiment and statistical γ rays cause those events[6].

Last, a run of data was acquired once the experiment was completed; as can be seen from fig.3.9, the background (β particles and γ rays) created in the target chamber during the experiment nicely decreases.

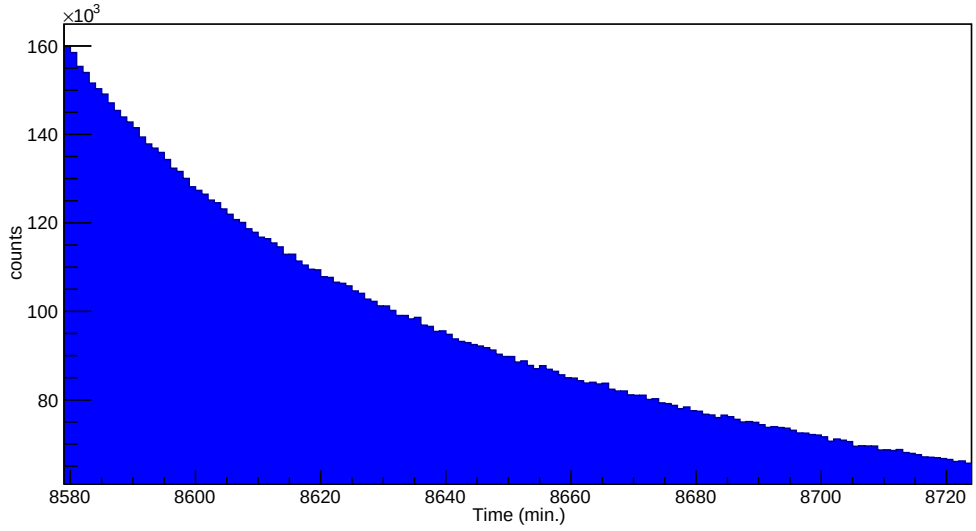

Figure 3.9. Background registered from JYUTube when the experiment was shut down.

[6]Other sources such as cosmic muons are also possible.

3.3 Summary and Discussion

A first test of the efficiency of the JYUTube to tag charged particles evaporated in fusion evaporation reactions and thus to select pure neutron evaporation reaction channels at MARA was run.

Even though signals are registered if no charged particles are emitted (approximately 20% from the ^{78}Kr(^{96}Mo, 4n)^{170}Pt channel), the JYUTube demonstrated the capability to tag one charged particle in about the 65% of cases and a probability about 80% to veto out two charged particles channels reaction.

The value for one charged particle tagging is calculated considering that the signals not coming from a charged particle in FOLD-1 and the events due to the detection of one charged particle present in FOLD-2.

Indeed, considering the ^{169}Ir channel events in tab.3.3, assuming the same percentage to fill FOLD-1 not due to a proton as for pure neutron evaporation channel ($\sim$10.6%), the estimation of the events in FOLD-1 due to proton decreases to 58%; however assuming that in the $\sim$ 6.3% of cases the FOLD-2 is filled even though no protons are expected, $\sim$345 events ($\sim$ 6.7% of 5152 total events) in FOLD-2 may be considered due to the detection of protons, whereby the net effect give a total detection efficiency for single proton evaporation is 65%.

Value for two protons channel is calculated in the same way considering the efficiency to detect at least one particle when two charged particles are evaporated.

On the other hand, another source of uncertainty for the measurement it is due to the effect shown in section 3.1.2: even if one radiation impinges on the detector, more than one signal is registered in the JYUTube. This phenomenon was confirmed during the run since several times neighbouring detectors registered signals once a high FOLD-N was filled, this can be explained with scattering of electrons among detector and cross-talk effect in the electronics.

Furthermore, the detection efficiency for γ rays shown in section 3.1.2 may explain the overall 20% of probability in the ^{78}Kr(^{96}Mo, 4n)^{170}Pt channel to register at least one count even though no charged particle has been evaporated in the reaction and thus pure neutron evaporation events are vetoed out[7]. This limitation could be overcome if the different types of impinging radiation could be distinguished, for example with a pulse shape analysis (PSA). Another possibility could be to tag γ rays coupling a germanium detector array with a large solid angle like JUROGAM II Germanium array around the target position. In this case, JYUTube could be also successfully used to tag charged particles evaporation reactions, since the events due to the detection of the γ rays can be removed.

[7]The γ emission is strongly dependent from the beam energy and the structure of the excited states of the nuclides itself. Moreover, due to the small number of events registered, the precision of the result is not high.

Due to the lack of capability to distinguish between α particles and protons of the detector and the low energy resolution reachable with MWDA the JYUTube in the present configuration can not be used to register the energy spectrum of the evaporated particles at the target position (see Appendix B).

Last, the aspect of degradation of the efficiency due to the radiation damage has to be considered. During the run no effects due to the radiation damage have been observed. In addition, an estimation can be done starting from the measurements in the paper [29], where the same scintillators were used. From the article, we can lead to the conclusion that the JYUTube can be used for years with the beam current used in our experiments without any observable damage (see Appendix C). On the other hand, radiation damages can occur to the SIPMs.

Conclusion and Outlook

A first measurement of the efficiency of the JYUTube to tag pure neutron evaporation channels in fusion evaporation reactions for nuclear spectroscopy at MARA was performed with a run in mass region 170. An efficiency of 65% to veto out one charged particle reaction channels and 80% for two charged particles was measured. On the other hand, the limitation to veto out pure neutron events one time over five was also registered.

However, performances of the JYUTube can be improved with further developments both on the hardware and the software. For example, one plan is to program the Lyrthec ADC-VHS to integrate the signals instead of apply the MWDA during the acquisition. With this improvement the energy resolution might enhance.

Moreover, integrators are planned to be added in order to shape the output signals from the JYUTube whereby PSA could be possible and thus to distinguish between different radiation impinged on the JYUTube.

In addition, since a CAD model of the JYUTube has been made by Mr. Juha Tuunanen, one development could be to use that model for simulation of the detection process, for example by input the CAD model in a program such as GEANT4.

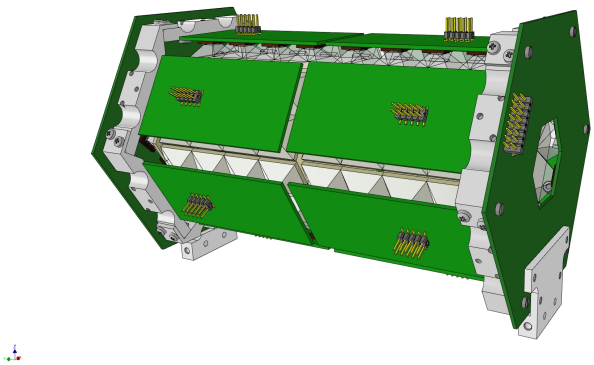

Figure 3.10. Computer Aided Design model of JYUTube made by Mr. Juha Tuunanen.

Further, by adding a summoner circuit at the output channels, signals from the JYUTube could be used in the TAC module to built the TOF histogram as in fig. 3.6.

Last, a systematic study of the energy response of the JYUTube to protons and α particles could be done using an accelerator capable to produce ions in the interesting region of energy for the evaporated particles (1 to 30 MeV) and a system capable to deliver bunches of single ions or low multiplicity of ions. the One example is the DEFEL beam line at LABEC [30].

Bibliography

[1] B. Blank and M. Borge, "Nuclear structure at the proton drip line: Advances with nuclear decay studies," *Progress in Particle and Nuclear Physics*, vol. 60, no. 2, pp. 403 – 483, 2008.

[2] http://nucleardata.nuclear.lu.se/toi/.

[3] M. Borge, "Beta-delayed particle emission," *Physica Scripta*, vol. 2013, no. T152, 2013.

[4] J. Uusitalo, *Private Communication*. February 2018. Department of Physics, University of Jyväskylä.

[5] D. D. Long, P. Richard, C. F. Moore, and J. D. Fox, "Coulomb displacement energies from isobaric analogue resonances," *Phys. Rev.*, vol. 149, pp. 906–912, Sep 1966.

[6] K. S. Krane, *Introductory nuclear physics*. New York, NY: Wiley, 1988.

[7] R. Bass, "Fusion of heavy nuclei in a classical model," *Nuclear Physics A*, vol. 231, no. 1, pp. 45–63, 1974.

[8] lise.nscl.msu.edu/pace4.html.

[9] LISE++group@NSCL/MSU, "Exotic beam production with fragment separators," 2013. http://lise.nscl.msu.edu/lise.html.

[10] G. F. Knoll, *Radiation detection and measurement; 4th ed.* New York, NY: Wiley, 2010.

[11] W. Leo, *Techniques for Nuclear and Particle Physics Experiments: A How-to Approach*. Springer, 1994.

[12] J. Birks, *The theory and practice of scintillation counting*. Pergamon Press, 1964.

[13] https://www.jyu.fi/science/en/physics/research/infrastructures/accelerator-laboratory.

[14] E. Liukkonen, "The jyväskylä's k130 cyclotron project." in Twelfth International Conference on Cyclotrons and their applications, Berlin, Germany, May 8-12, 1989.

[15] R. Geller, *Electron Cyclotron Resonance Ion Sources and ECR Plasmas*. London: IOP Publishing, 1996.

[16] P. Heikkinen, *Private Communication*. May 2018. Department of Physics, University of Jyväskylä.

[17] *CAS - CERN Accelerator School : 5th General Accelerator Physics Course*, (Geneva), CERN, 1994. p.805.

[18] https://www.jyu.fi/science/en/physics/research/infrastructures/accelerator-laboratory/nuclear-physics-facilities/recoil-separators/mara-mass-analysing-recoil-apparatus.

[19] J. Sarén, *The ion-optical design of the MARA recoil separator and absolute transmission measurements of the RITU gas-filled recoil separator*. PhD thesis, University of Jyväskylä, 2011.

[20] SenseL, "Smt, c-series." https://sensl.com/products/c-series/.

[21] ELJEN. https://eljentechnology.com/products/plastic-scintillators/ej-200-ej-204-ej-208-ej-212.

[22] J. Kantele, *Handbook of Nuclear Spectrometry*. Academic Press, 1995.

[23] J. F. Ziegler, M. D. Ziegler, and J. P. Biersack, "Srim - the stopping and range of ions in matter (2010)," *Nuclear Instruments and Methods in Physics Research B*, vol. 268, pp. 1818–1823, 06 2010.

[24] A. Georgiev, W. Gast, and R. Lieder, "Analog-to-digital conversion based on a moving window deconvolution," vol. 41, pp. 1116 – 1124, 09 1994.

[25] DaresburyLaboratory, "Midas, the multi instance data acquisition system." http://npg.dl.ac.uk/MIDAS/.

[26] http://www.nndc.bnl.gov/nudat2/.

[27] P. Rahkila, "Grain—a java data analysis system for total data readout," *Nuclear Instruments and Methods in Physics Research Section A: Accelerators, Spectrometers, Detectors and Associated Equipment*, vol. 595, pp. 637–642, 11 2007.

[28] R. Brun and F. Rademakers, "Root — an object oriented data analysis framework," *Nuclear Instruments and Methods in Physics Research Section A: Accelerators, Spectrometers, Detectors and Associated Equipment*, vol. 389, no. 1, pp. 81 – 86, 1997. New Computing Techniques in Physics Research V.

[29] H. Jivan, E. Sideras-Haddad, R. Erasmus, S. Liao, M. Madhuku, G. Peters, K. Sekonya, and O. Solvyanov, "Radiation hardness of plastic scintillators for

the tile calorimeter of the atlas detector," *Journal of Physics: Conference Series*, vol. 645, no. 1, 2015.

[30] A. Castoldi, C. Guazzoni, D. Mezza, G. V. Montemurro, L. Carraresi, and F. Taccetti, "Upgrade of the defel proton beam line for detector response mapping," *2013 IEEE Nuclear Science Symposium and Medical Imaging Conference (2013 NSS/MIC)*, pp. 1–5, 2013.

[31] R. Evans, *The atomic nucleus*. New York: McGraw Hill Book Company, Inc., 1955.

Appendix A

Calculation of Nichel foils thickness on JYUTube detectors

As already explained in section 1.2, scattered particles both from the target and the beam can reach the JYUTube detector at the target position.

In order to avoid those particles to be detected, Nichel foils can added on the JYUTube as said in section 3.2. However foils do not have to be thick enough to stop the evaporated particles. Thickness can be calculated according with the Bethe-Block formula using SRIM software [23].

Some examples of calculation for the reaction 3.2 and reported in the following tables.

Table A.1. Averages of the ranges of Krypton nuclei in Ni.

Krypton Energy (MeV)	Range (μm)
50	4.4
100	6.5
200	10
300	14
390	17

Table A.2. Averages of ranges of protons in Ni.

Proton Energy (MeV)	Range (μm)
3	32
10	231
20	756

Remembering that the most energetic particles are emitted forward in the laboratory frame, as can be seen the range of Kr ions with the maximum energy is lower than

Table A.3. Averages of ranges of α particles in Ni.

α Energy (MeV)	Range (μm)
5	9.3
10	24.9
20	73.8

the range of α particles and protons of higher energy, and this property can be assumed for all the angles. For this reason the Ni foils placed can stop the scattered particles but not fully stop protons and α. However, these evaporated particles partially release their energy in the Ni foils, as a result the energy spectrum from is altered from this effect. Since the energy of the scattered particles is strongly dependent on the reaction parameters, these calculations have to repeated for each reaction in order to install Ni foils of the suitable thickness.

Appendix B

Information on the fusion evaporation reaction from the JYUTube

As already discussed in section 3.3, in the current configuration the JYUTube can not provide an energy spectrum of the evaporated particles at the target position. This limitation is clearly visible from fig.B.1. By using PACE4 program it is possible to

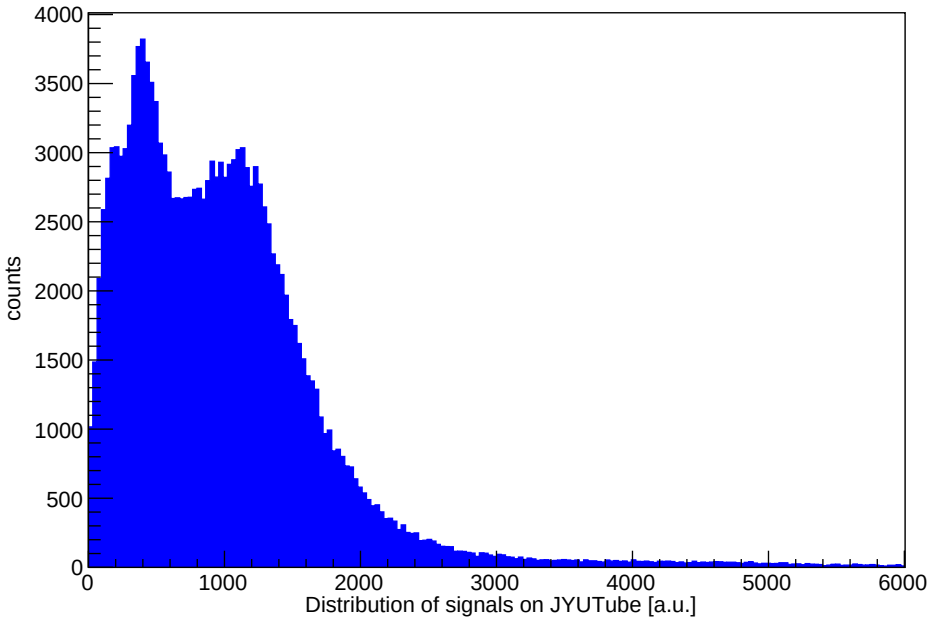

Figure B.1. Distribution of events from JYUTube correlated with the fusion recoil events in DSSD.

obtain energy spectra for evaporated particles. Examples for α particles and protons

are presented in fig.B.3.

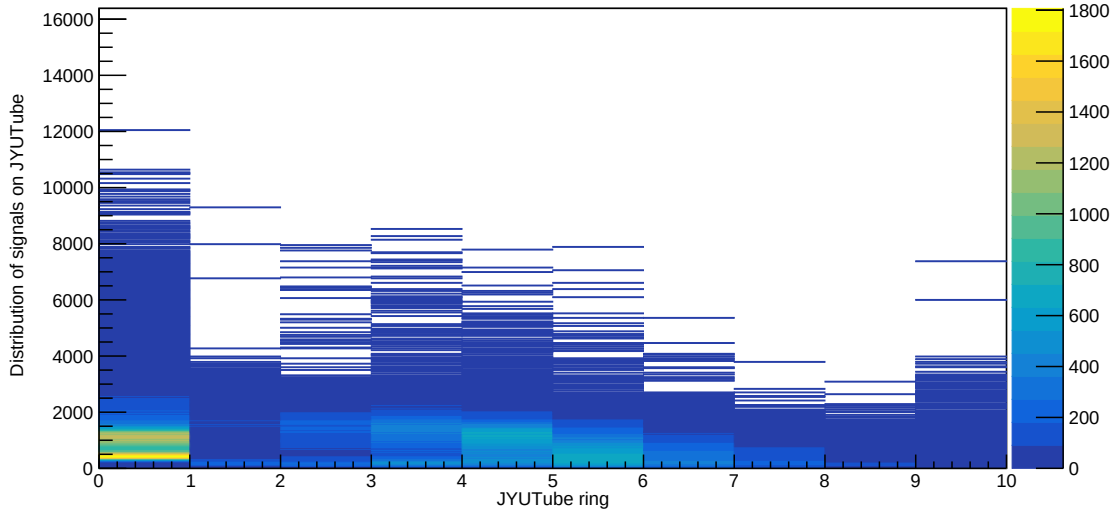

Figure B.2. Distribution of signals from JYUTube correlated with the tube rings.

This limitation is due to several factors, that are

- the resolution of the EJ200 detectors, as measured in section 3.1;
- the release of energy of the particles in the Ni foils and in the aluminized Mylar placed on the crystals;
- the MWDA used during the acquisition, as visible in section 3.1.

However, with further analysis, the distribution was related with the rings of the JYUTube. As presented in fig.B.2, an increasing of the average of the distribution with the angle is visible, as expected.

For this reason, once some of the improvements presented in the conclusion will be done, maybe also some information on the reactions could be extracted from the JYUTube.

For an exhaustive treatment of the interaction of radiation with matter Evans [31] can be consulted.

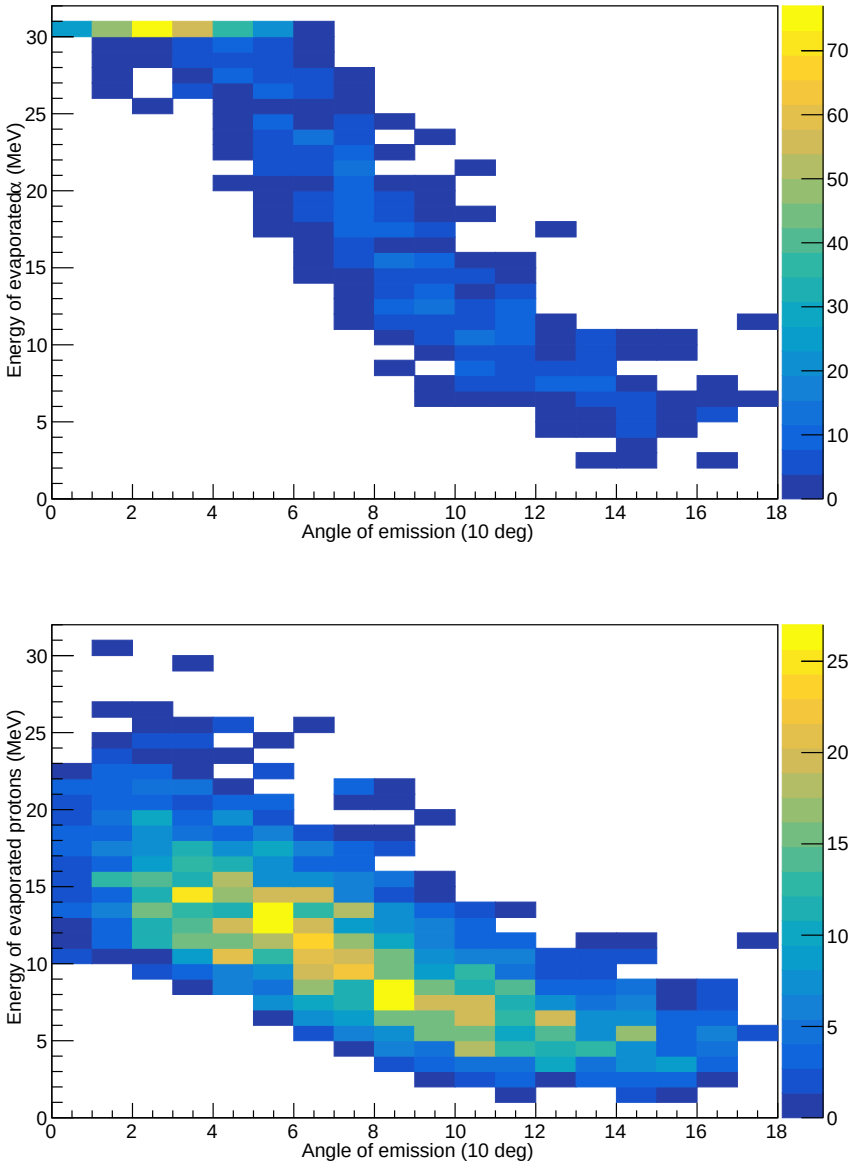

Figure B.3. Energy of α particles (top) and protons (bottom) evaporated for reaction 3.2 at 390 MeV from simulations with PACE4 software.

Appendix C

Radiation robustness for EJ200 scintillators

In article [29] EJ200 scintillators are used for Tile Calorimeter of the ATLAS detector. The authors measured that for the dose of 0.8 MGy "no structural damage occurs and light loss can be attributed to a breakdown in the light transfer between base and fluor dopants."

By using this value, and calculating the dose received from the JYUTube, an estimation of the beam time needed to degrade the detector can be done. The unit of dose is defined as the ratio between the energy released in a certain mass and the mass itself, consequently one Gray is defined as

$$\mathrm{Gy} = \frac{\mathrm{J}}{\mathrm{Kg}}. \tag{C.1}$$

In order to calculate the energy released in the JYUTube by the particles evaporated, we can consider the rates registered and an average energy of 10 MeV. The mass is calculated starting from the density and the volume of each scintillator. Rates were 25 thousands counts per second, the density is $\rho = 1.023 \frac{\mathrm{g}}{\mathrm{cm}^{-3}}$. Thus

$$\frac{\mathrm{Dose}}{s} = \frac{1.6 \cdot 10^{-12} \cdot 25 \cdot 10^{3} \mathrm{J}}{120 \cdot 0.8 \cdot 1.023 \cdot 10^{-3} \mathrm{Kg}} \sim \frac{4 \cdot 10^{-8} \mathrm{Gy}}{s}. \tag{C.2}$$

Since one year is $\sim 10^7$ s, after one year the total dose is about 1 Gy. Obviously, since the emission of the particles is not symmetric, this is an average value, however it is six order of magnitude lower than the value indicated in the article.

Acknowledgements

I would like to thank:

prof. Andrea Stefanini, who kicked off my Master's Programme;

the MARA people for their help, in particular Dr. Jan Sarén, Dr. Panu Ruotsalainen and Mr. Jari Partanen. A special acknowledgement to Dr. Ulrika Forsberg;

the administrative staff for its support, in particular Ms. Minttu Happaniemi;

the Head of the Department, that has provided me a grant during my Master's Programme;

the students of physics that have accompanied me in these two years. Particularly, the master's seminar group;

Dr. Pauli Heikkinen, since it is always worth to speak with him;

my "cuddly and plumpy muggle" in Cambridgeshire;

lastly Dr. Juha Uusitalo, for offering me this project.